**Supporting information**

**Spin evolution and flip in oxygen reduction reaction: a detailed theoretical study on Cu(Ni)XP$_2$S$_6$ (X = In, Bi and Cr)**

*Haoyun Bai[1], Di Liu[1], Pengfei Zhou[1], Jinxian Feng[1], Xulei Sui[3], Yunhao Lu[4], Hongchao Liu[1]\*, and Hui Pan[1,2]\**

[1] Institute of Applied Physics and Materials Engineering, University of Macau, Macao SAR, 999078, P.R. China

[2] Department of Physics and Chemistry, Faculty of Science and Technology, University of Macau, Macao SAR, 999078, P. R. China

3 Shenzhen Key Laboratory of Special Functional Materials, Shenzhen Engineering Laboratory for Advance Technology of Ceramics, Guangdong Research Center for Interfacial Engineering of Functional Materials, College of Materials Science and Engineering, Shenzhen University, Shenzhen, 518060, P. R. China

4 Department of Physics, Zhejiang University, Hangzhou, 310027, China

\*Corresponding Authors

H. Liu: hcliu@um.edu.mo (email)

H. Pan: huipan@um.edu.mo (email), +853 88224427 (tel.), +853-88222454 (fax)

**Supplementary tables**

Table S1. The calculated total energy (E$_0$), formation energy (E$_f$), lattice constant (a), thickness (t) and phase transition barrier of polarization reverse (E$_b$) for the primitive cells of CuInP$_2$S$_6$ (CIPS), CuBiP$_2$S$_6$ (CBPS) and CuCrP$_2$S$_6$ (CCPS).

| | E$_0$ | E$_f$ (eV) | a (Å) | t (Å) | E$_b$ (eV) |
|---|---|---|---|---|---|
| **CIPS** | -45.18 | -3.37 | 6.16 | 3.41 | 0.34 |
| **CBPS** | -45.97 | -2.83 | 6.34 | 3.50 | 0.33 |
| **CCPS** | -52.17 | -3.41 | 5.95 | 3.15 | 0.12 |

Table S2. The calculated total energies in different states, exchange energy ($E_{ex}$) between FM and AFM states for the 2×2×1 supercells of $CuInP_2S_6$ (CIPS), $CuBiP_2S_6$ (CBPS) and $CuCrP_2S_6$ (CCPS). $E_{ex}$ is calculated as $E_{ex} = E_{FM} - E_{AFM}$.

| | Energy of state (eV) | | | | $E_{ex}$ (meV) |
|---|---|---|---|---|---|
| | AFE | FE | FE_AFM | FE_FM | |
| CIPS | -180.91 | -180.72 | -180.72 | -180.72 | 0 |
| CBPS | -183.92 | -183.86 | -183.86 | -183.86 | 0 |
| CCPS | -203.38 | -203.01 | -208.62 | -208.69 | 70.09 |

Table S3. The calculated total energy ($E_0$) and doping energy ($E_d$) for Ni-doped 2×2×1 supercell of $CuInP_2S_6$ (CNIPS), $CuBiP_2S_6$ (CNBPS) and $CuCrP_2S_6$ (CNCPS). CNCPS (parallel): the magnetic moment of Ni is parallel to that of Cr.

| | $E_0$ (eV) | $E_d$ (eV) | $E_d$ (J·m$^{-2}$) | a (Å) | t (Å) |
|---|---|---|---|---|---|
| CNIPS | -181.65 | 0.81 | 0.0993 | 12.31 | 3.46 |
| CNBPS | -184.79 | 0.81 | 0.0943 | 12.67 | 3.55 |
| CNCPS | -209.64 | 0.79 | 0.1045 | 11.88 | 3.28 |
| CNCPS (parallel) | -209.49 | | | | |

Table S4. The calculated Gibbs free energies (G), total magnetic moment (magmom), Gibbs free energy change (ΔG) between two reaction steps (e.g., * → *OO, ΔG = -0.34 eV on CNIPS), and magnetic moment of ion during the ORR reaction.

**CNIPS**

| step | G (eV) | magmom ($\mu_B$) | ΔG (eV) | magmom of ion ($\mu_B$) | | | | |
|---|---|---|---|---|---|---|---|---|
| | | | | Ni | O1 | O2 | H1 | H2 |
| * | -187.53 | ±1.00 | -1.19 | ±1.00 | | | | |
| *O2 | -197.79 | ±1.00 | -0.34 | ∓0.03 | ±0.48 | ±0.38 | | |
| *OOH (g) | -201.74 | ±2.00 | -0.54 | ±1.12 | ±0.42 | ±0.10 | ±0.005 | |
| *OOH (e) | -201.49 | 0.00 | -0.30 | -0.30 | 0.12 | 0.14 | -0.006 | |
| *O (g) | -192.49 | ±3.00 | -1.48 | ±1.36 | ±0.99 | | | |
| *O (e) | -192.00 | ±1.00 | -0.99 | ±0.31 | ±0.55 | | | |
| *OHOH | -205.55 | 1.00 | -0.40 | 0.872 | 0.01 | 0.06 | 0.000 | 0.000 |
| *OH (g) | -197.26 | ±2.00 | -1.37 | ±1.21 | ±0.35 | | 0.00 | |
| *OH (e) | -197.07 | 0.00 | -1.18 | ±0.03 | ±0.02 | | 0.00 | |

**CNBPS**

2

| step | G (eV) | magmom (μB) | ΔG (eV) | magmom of ion (μB) | | | | |
|---|---|---|---|---|---|---|---|---|
| | | | | Ni | O1 | O2 | H1 | H2 |
| * | -190.41 | ±1.00 | -1.24 | ±1.00 | | | | |
| *O2 | -200.69 | ±1.00 | -0.36 | ±0.02 | ±0.37 | ±0.47 | | |
| *OOH (g) | -204.64 | ±2.00 | -0.55 | ±1.12 | ±0.42 | ±0.10 | ±0.004 | |
| *OOH (e) | -204.40 | 0.00 | -0.30 | 0.28 | -0.15 | -0.12 | 0.006 | |
| *O (g) | -195.34 | ±3.00 | -1.43 | ±1.35 | ±0.99 | | | |
| *O (e) | -194.87 | ±1.00 | -0.95 | ±0.33 | ±0.556 | | | |
| *OHOH | -208.35 | 1.00 | -0.30 | 0.870 | 0.06 | 0.01 | 0.000 | 0.000 |
| *OH (g) | -200.10 | ±2.00 | -1.35 | ±1.21 | ±0.34 | | ∓0.001 | |
| *OH (e) | -199.94 | 0.00 | -1.19 | -0.052 | 0.021 | | 0.000 | |

**CNCPS**

| step | G (eV) | magmom (μB) | ΔG (eV) | magmom of ion (μB) | | | | |
|---|---|---|---|---|---|---|---|---|
| | | | | Ni | O1 | O2 | H1 | H2 |
| * | -216.92 | 11.00 | -1.51 | -1.00 | | | | |
| *O2 | -226.74 | 11.00 | 0.09 | -0.05 | -0.33 | -0.40 | | |
| *O2 | -226.76 | 13.00 | 0.07 | 0.02 | 0.43 | 0.53 | | |
| *OOH (g) | -230.74 | 10.00 | -0.57 | -1.09 | -0.40 | -0.09 | -0.005 | |
| *OOH (e) | -230.65 | 14.00 | -0.49 | 1.14 | 0.41 | 0.10 | 0.005 | |
| *OOH (e) | -230.44 | 12.00 | -0.27 | -0.25 | 0.15 | 0.11 | -0.006 | |
| *O (g) | -221.53 | 9.00 | -1.52 | -1.32 | -0.97 | | | |
| *O (e) | -221.43 | 15.00 | -1.41 | 1.37 | 0.99 | | | |
| *O (e) | -221.06 | 11.00 | -1.04 | -0.25 | -0.49 | | | |
| *O (e) | -220.97 | 13.00 | -0.96 | 0.59 | 0.31 | | | |
| *OHOH | -234.43 | 11.00 | -0.28 | -0.84 | -0.06 | -0.01 | 0.000 | 0.000 |
| *OHOH | -234.42 | 13.00 | -0.27 | 0.87 | 0.06 | 0.01 | 0.000 | 0.000 |
| *OH (g) | -226.33 | 10.00 | -1.50 | -1.17 | -0.32 | | 0.001 | |
| *OH (e) | -226.41 | 14.00 | -1.27 | 1.22 | 0.34 | | -0.001 | |
| *OH (e) | -225.94 | 12.00 | -1.11 | 0.58 | 0.14 | | 0.000 | |

Note: the Gibbs free energies are calculated based on the ground state of the previous step. (g) and (e) represent excited and ground states, respectively.

Table S5. The calculated Gibbs free energies for the adsorptions of $H^+$, $OH^-$ and $H_2O$ on CNXPS (unit: eV).

| | CNIPS | CNBPS | CNCPS |
|---|---|---|---|
| **H** | 0.34 | 0.36 | 0.71 |
| **OH** | 0.86 | 0.89 | 1.12 |
| **H₂O** | 0.19 | 0.04 | 0.53 |

Table S6. Summary of the representative ORR performance in literatures. The overpotential is defined as $\eta_{ORR}=max(\Delta G_i)/e + 1.23$ in DFT calculation, and the voltage at -1 mA/cm$^2$ in the experiment.

| Electrocatalyst | Type | Overpotential (V) | Ref |
| --- | --- | --- | --- |
| Pt (111) | DFT/novel metal | 0.45 | 1 |
| Pt | Experiment/novel metal | 0.38 | 2 |
| Fe-ODAN-1% | Experiment/metal based | 0.47 | 2 |
| $Ba_{0.5}Sr_{0.5}Co_{0.8}Fe_{0.2}O_{3-d}$ | Experiment/metal compound | -0.25 | 3 |
| N, P, S co-doped hollow carbon polyhedron | Experiment/SAC | 0.37 | 4 |
| Fe-SAs/NPS-HC | Experiment/SAC | 0.37 | 4 |
| Fe$^{II}$-N/C | Experiment/SAC | 0.33 | 5 |
| NiS | Experiment/metal compound | 0.66 | 6 |
| CoCuMnO$_x$ | Experiment/metal compound | 0.85 | 7 |
| Fe/Ni–N–C | Experiment/DAC | 0.32 | 8 |
| Fe/Ni–N–C | DFT/DAC | 0.22 | 8 |
| Co-C$_4$N$_4$ | DFT/SAC | 0.64 | 9 |
| Pd-C$_3$N$_4$ | DFT/SAC | 0.95 | 10 |
| Ag-C$_3$N$_4$ | DFT/SAC | 0.81 | 10 |
| FeN$_4$-Graphene | DFT/SAC | 0.74 | 11 |
| Ag$_4$/C$_2$N | DFT/novel metal | 0.31 | 12 |
| Co-C$_{24}$N$_{24}$ | DFT/metal based | 0.83 | 13 |
| Cu(Ni)CrP$_2$S$_6$ | DFT/metal compound | 0.66 | This work |

Table S7. Gibbs free energy (G) of O$_2$, H$_2$ and H$_2$O. unit: eV.

| | G |
| --- | --- |
| O$_2$ | -9.91 |
| H$_2$ | -6.82 |
| H$_2$O | -14.14 |

**Supplementary Figures**

Stability and physical properties
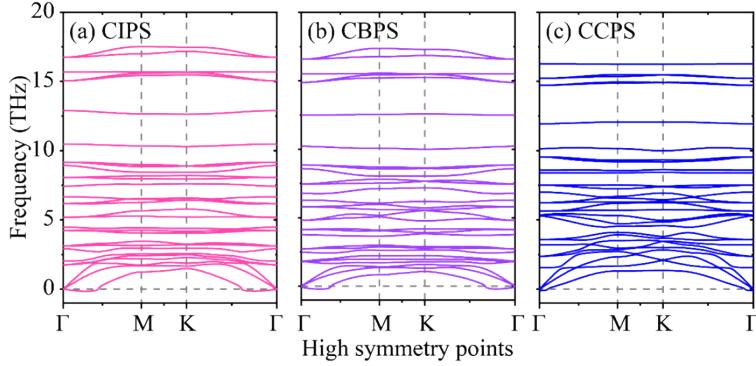


Figure S1. The calculated phonon dispersions of (a) $CuInP_2S_6$, (b) $CuBiP_2S_6$ and (c) $CuCrP_2S_6$.
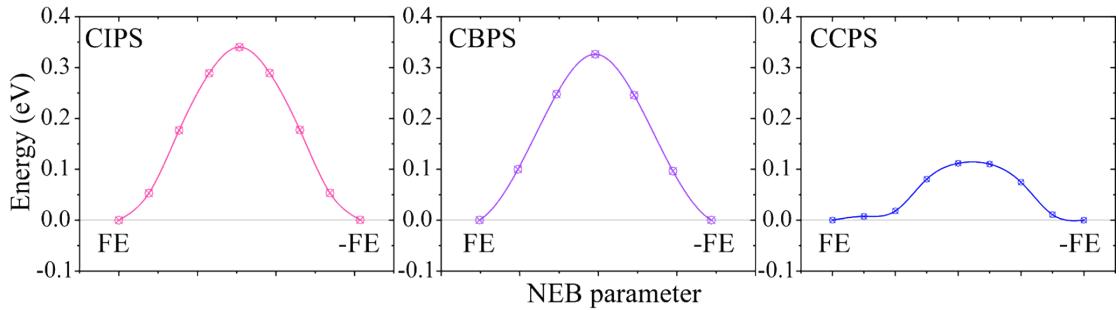


Figure S2. The minimum energy pathway in the polarization reverse process for (a) $CuInP_2S_6$, (b) $CuBiP_2S_6$ and (c) $CuCrP_2S_6$.
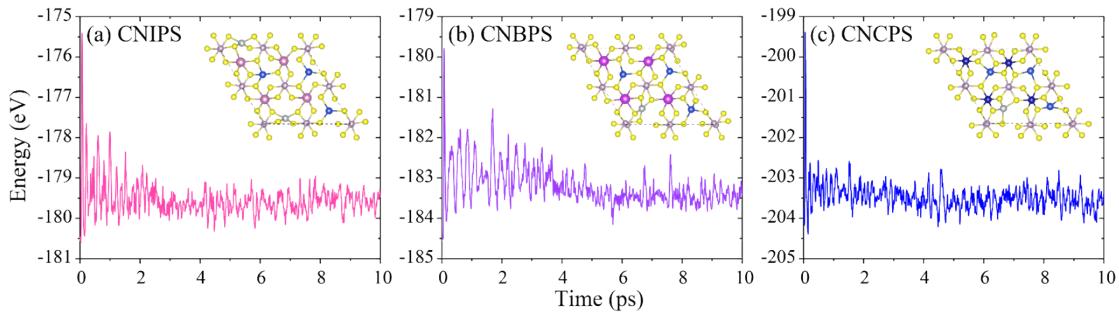


Figure S3. The *ab initio* molecular dynamics (AIMD) simulations for Ni doped (a) $CuInP_2S_6$ (CNIPS), (b) $Ni-CuBiP_2S_6$ (CNBPS) and (c) $Ni-CuCrP_2S_6$ (CNCPS).
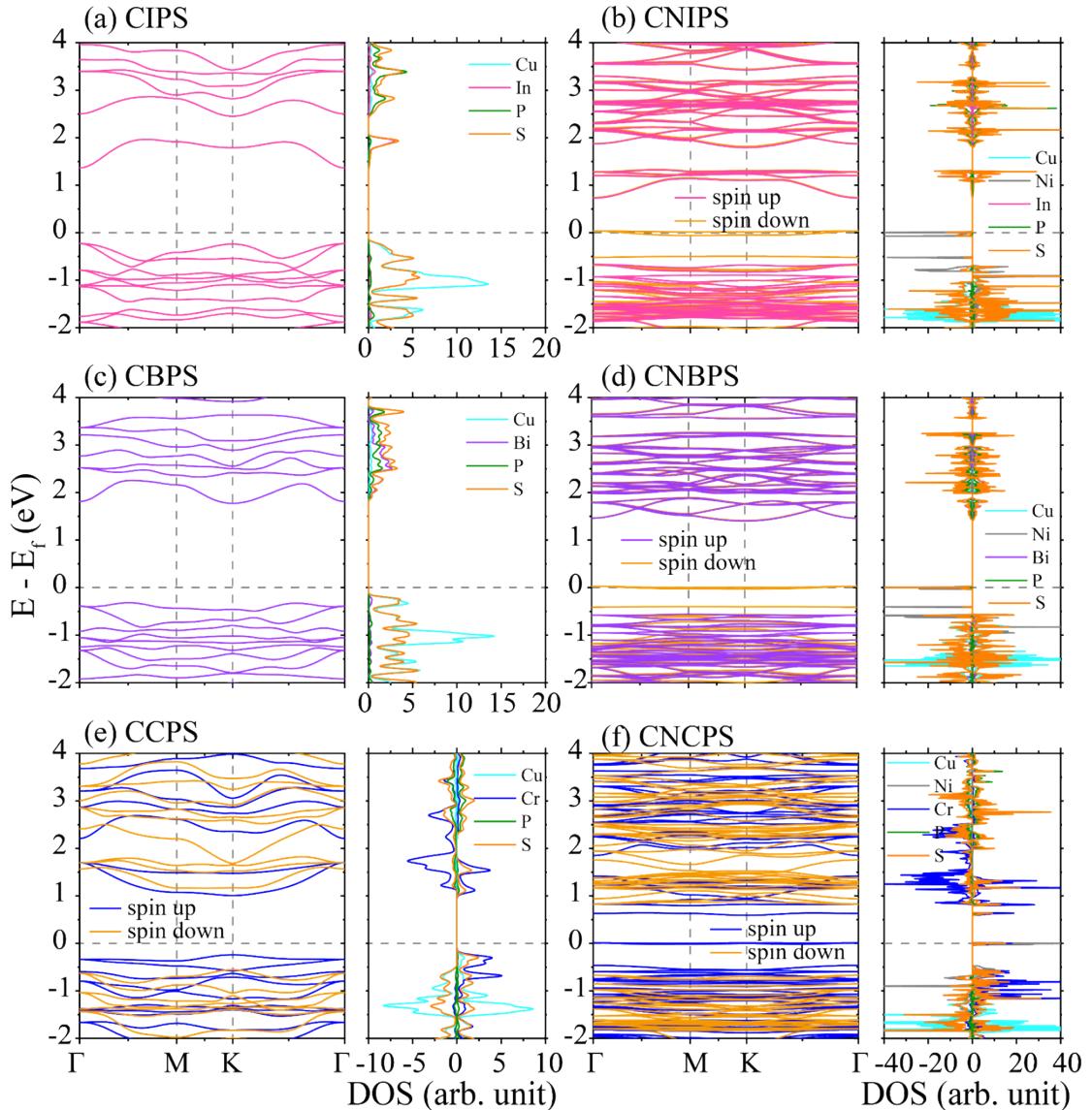
Figure S4. The band structures and partial densities of states (PDOSs) of (a) CIPS, (b) CBPS, (c) CCPS, (d) CNIPS, (e) CNBPS and (f) CNCPS.
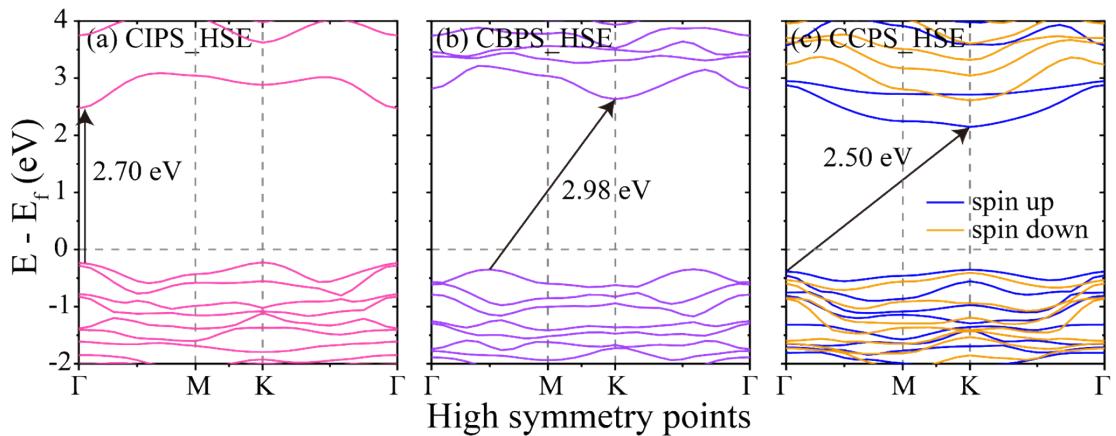


Figure S5. Band structures of (a) CIPS, (b) CBPS and (c) CCPS calculated by

HSE06.

Active sites and $O_2$ adsorption
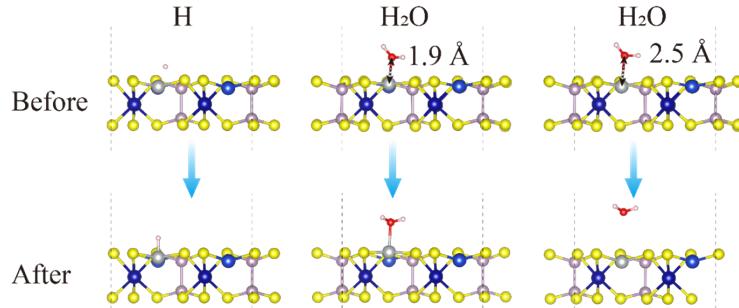


Figure S6. Adsorption of H and $H_2O$ on the surface of CNXPS.
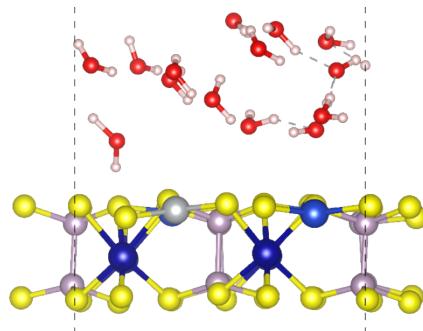


Figure S7. The final structure of AIMD simulation for a $H_2O$ layer on the surface of CNCPS.
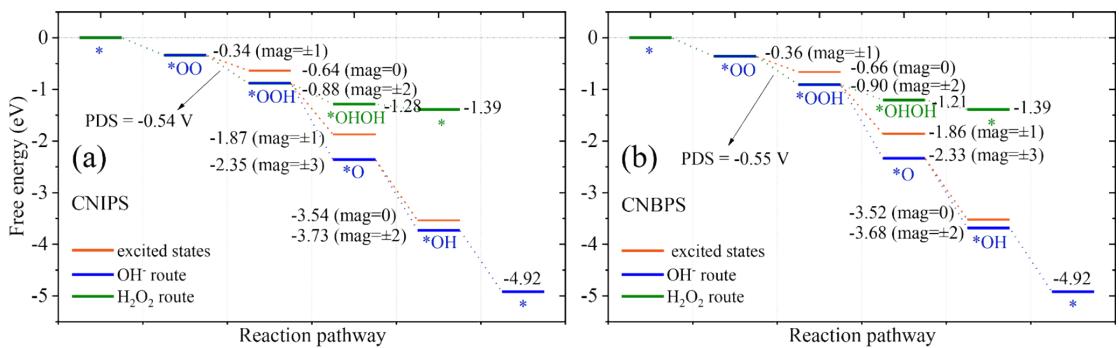


Figure S8. The diagrams of Gibbs free energy change in the ORR process for (a) CNIPS and (b) CNBPS.
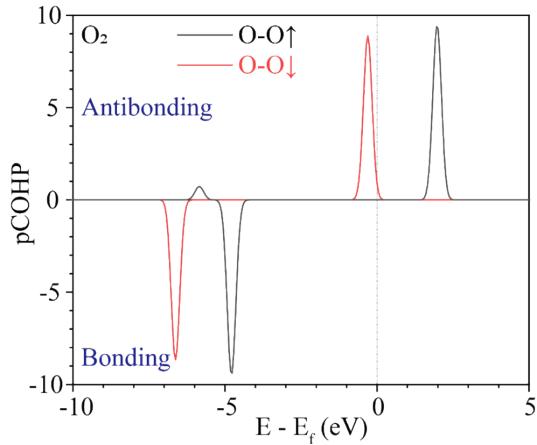
Figure S9. The Crystal orbital Hamilton populations (COHP) analysis for $O_2$. The ground state shows a magnetic moment of -2 $\mu_B$.
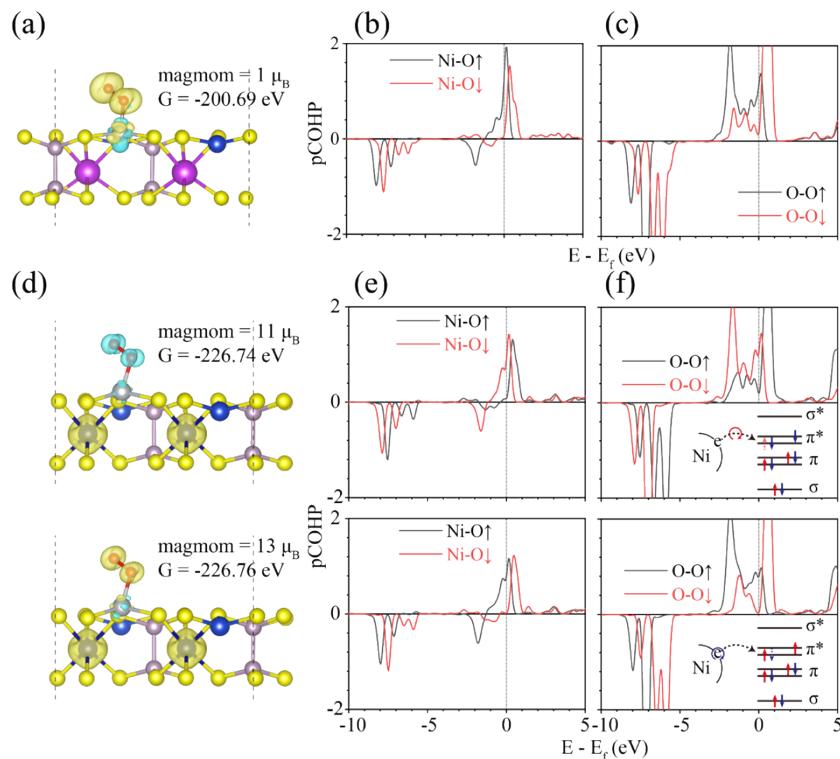


Figure S10. (a) Spin density and COHP analysis for (b) Ni-O and (c) O-O bond of CNBPS-*OO. (d) Spin density, and COHP analysis for (e) Ni-O and (f) O-O bond of CNCPS-*OO (+11) (up) and CNCPS-*OO (+13) (down). In (a) and (d), the yellow and cyan represents spin-up and spin-down, respectively. Both isosurfaces in (a) and (d) are 0.02 e/$Å^3$.
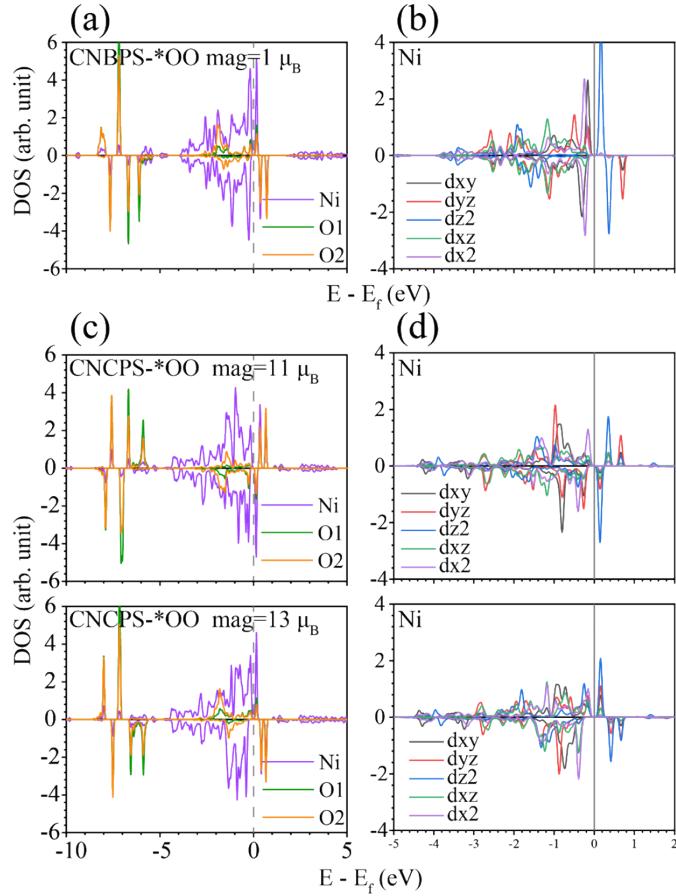
Figure S11. PDOSs for (a) Ni, O1 and O2 atoms and (b) *d* orbitals of Ni in CNBPS-*OO. PDOSs for (c) Ni, O1 and O2 atoms and (d) *d* orbitals of Ni in CNCPS-*OO (+11) and CNCPS-*OO (+13).
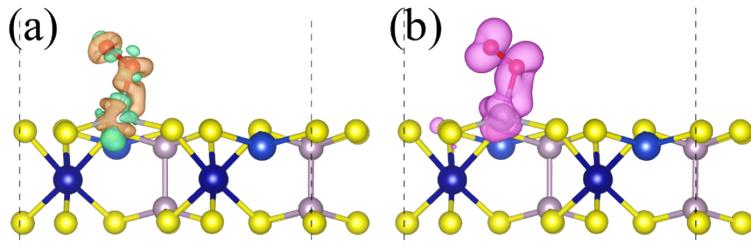


Figure S12. (a) Differential charge and (b) differential spin densities of CNCPS-*OO (+11). The orange and green denote charge accumulation and loss, respectively. The pink and blue indicate that the magnetic moment gets bigger and smaller, respectively. Both isosurfaces in (a) and (b) are 0.005 e/Å³.

CNXPS-*OOH intermediate
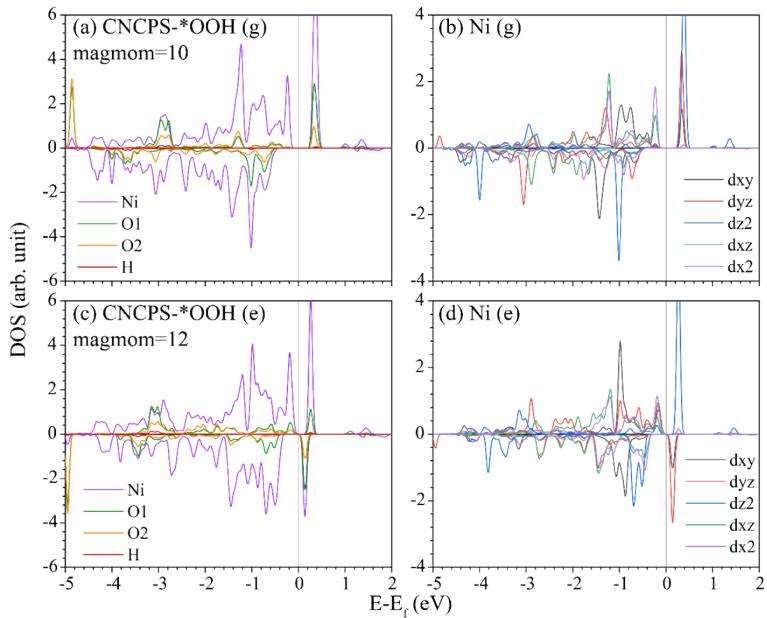


Figure S13. PDOSs for (a) Ni, O1, O2 and H atoms and (b) *d* orbitals of Ni for ground-state CNCPS-*OOH (+10). PDOSs for (c) Ni, O1 and O2 atoms and (d) *d* orbitals of Ni for excited-state CNCPS-*OOH (+12).
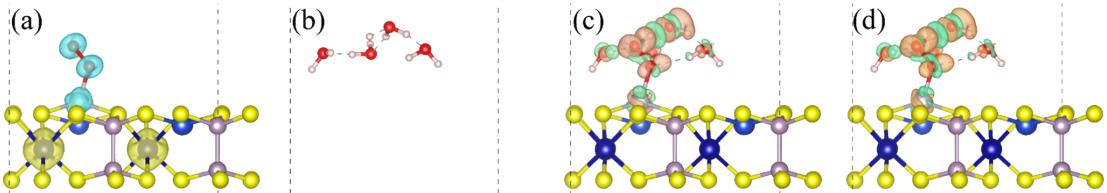


Figure S14. Spin densities of (a) CNCPS-*OO$^-$ and (b) $H_9O_4^+$. The yellow and cyan represents spin-up and spin-down, respectively. Both isosurfaces in (a) and (b) are 0.02 e/Å$^3$. Differential charge densities of (c) ground-state CNCPS-*OOH+$H_9O_4$ (+10) and (d) excited-state CNCPS-*OOH+$H_9O_4$ (+12). The orange and green denote the charge accumulation and loss, respectively. Both isosurfaces in (a) and (b) are 0.005 e/Å$^3$.
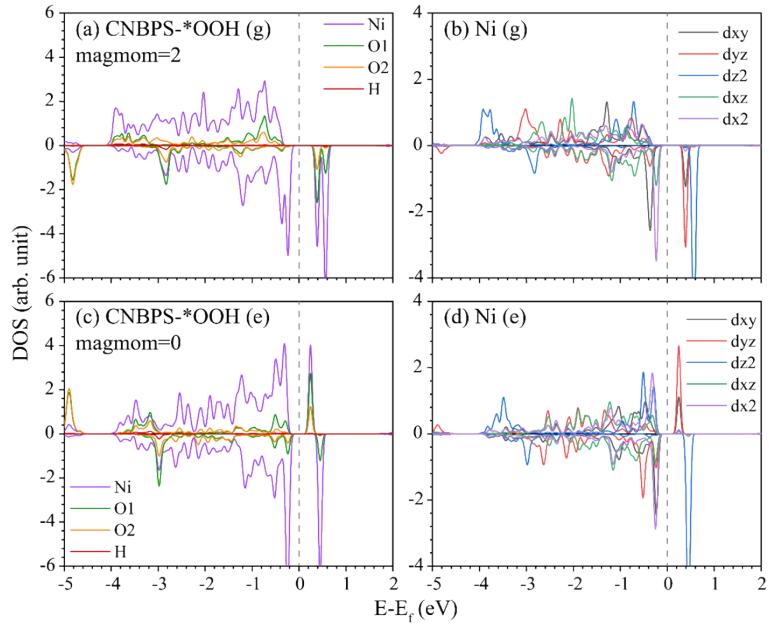
Figure S15. PDOSs for (a) Ni, O1, O2 and H atoms and (b) *d* orbitals of Ni for ground-state CNBPS-*OOH (+2). PDOSs for (c) Ni, O1 and O2 atoms and (d) *d* orbitals of Ni for CNBPS-*OOH in excited-state CNBPS-*OOH (0).
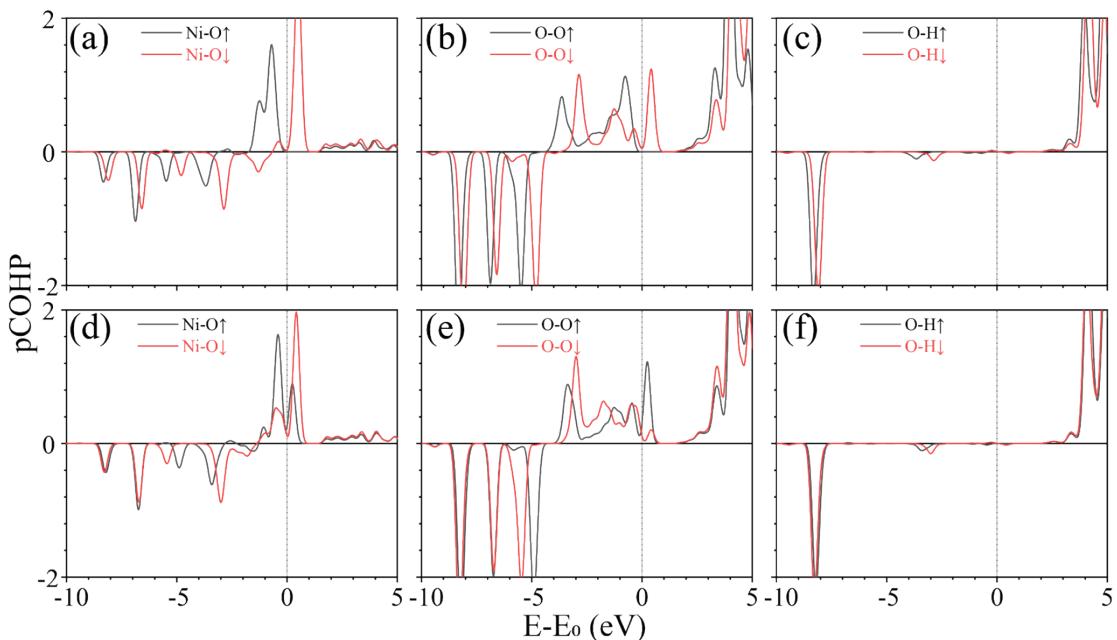


Figure S16. COHP analysis for (a) Ni-O, (b) O-O and (c) O-H bond of ground-state CNBPS-*OOH (±2). COHP analysis for (d) Ni-O, (e) O-O and (f) O-H bond of ground-state CNBPS-*OOH (0).

CNXPS-*O and CNCPS-*H$_2$O$_2$ intermediate
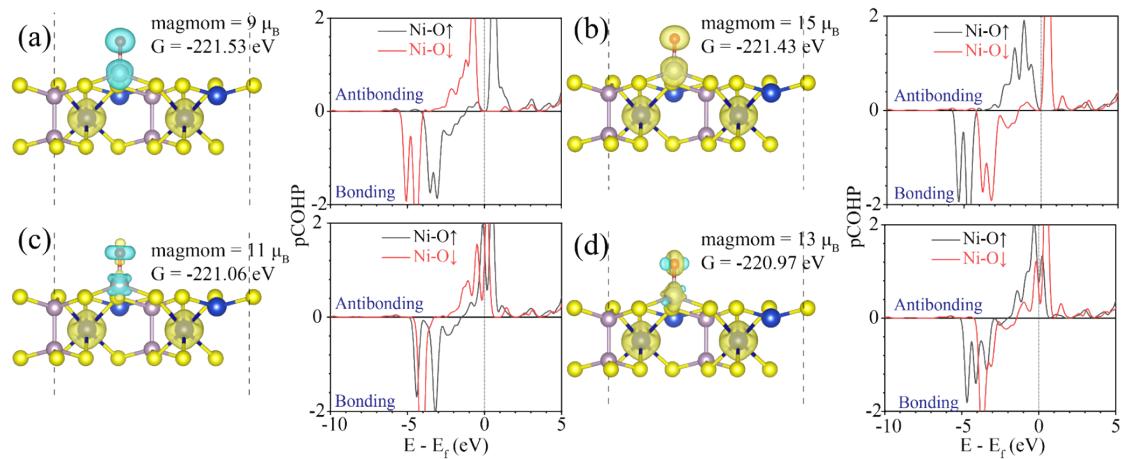


Figure S17. Spin density and COHP analysis of Ni-O bond in different states. The yellow and cyan represents spin up and down, respectively. Isosurfaces are 0.02 e/Å$^3$.
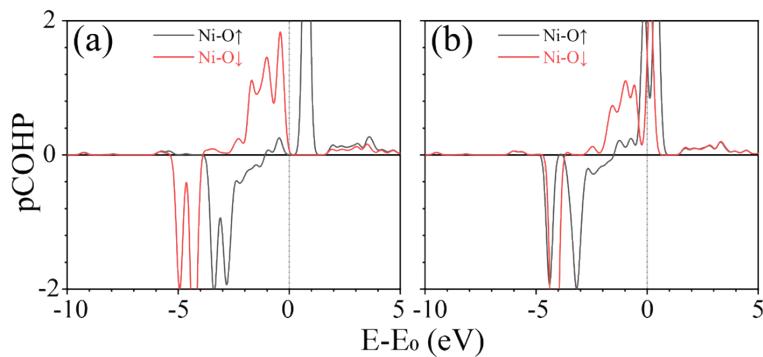


Figure S18. COHP analysis for Ni-O bond of (a) ground-state CNBPS-*O (±3) and (b) excited-state CNBPS-*O (±1).
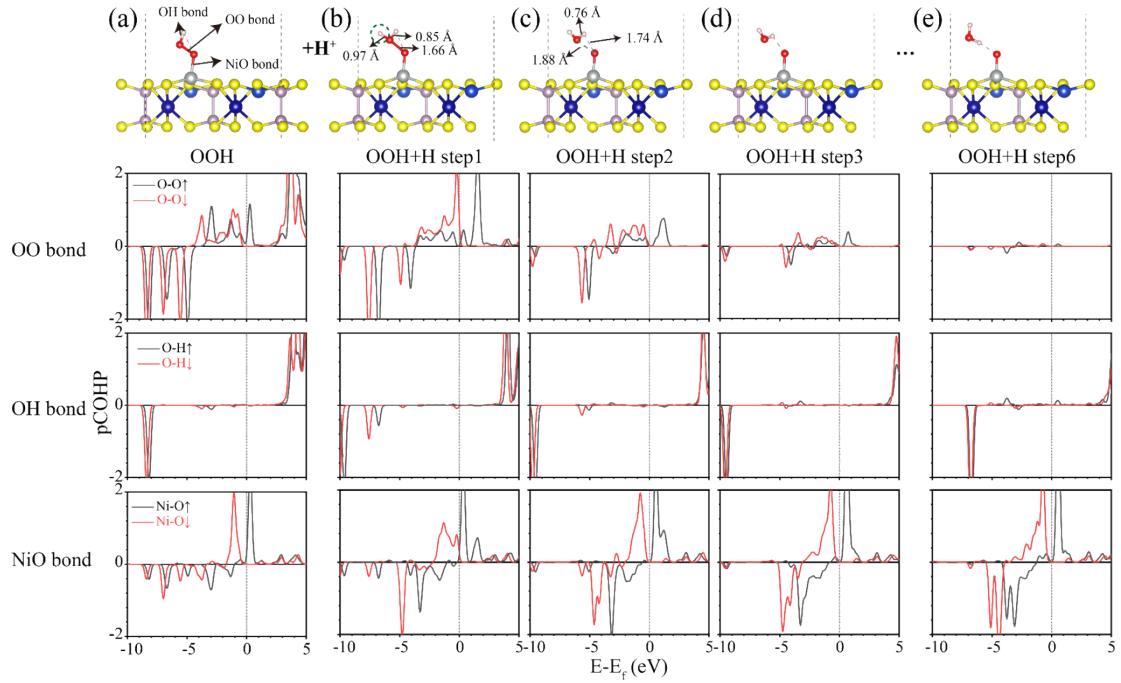
Figure S19. Structure and COHP analysis for O-O, O-H and Ni-O bonds of (a) CNCPS-*OOH, (b-d) ground state of CNCPS-*OOH+$H_9O_4$ during NEB route and (e) ground state of final state of CNCPS-*OOH+$H_9O_4$. We only show H adsorbed on O2 for a clear display.
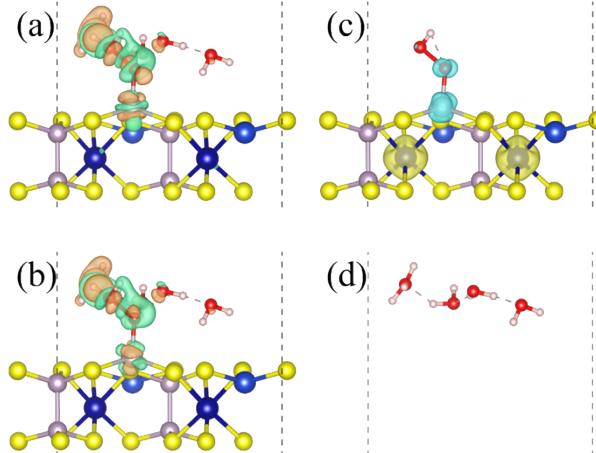


Figure S20. Differential charge density of (a) ground-state CNCPS-*OOH+$H_9O_4$ (+9) and (b) excited-state CNCPS-*OOH+$H_9O_4$ (+11). The orange and green denote charge accumulation and loss, respectively. Spin density of (c) CNCPS-*OOH$^-$ and (d) $H_9O_4^+$. The yellow and cyan represents spin up and down, respectively. Isosurfaces are 0.005 e/Å$^3$ in (a-b), and 0.02 e/Å$^3$ in (c-d).

13
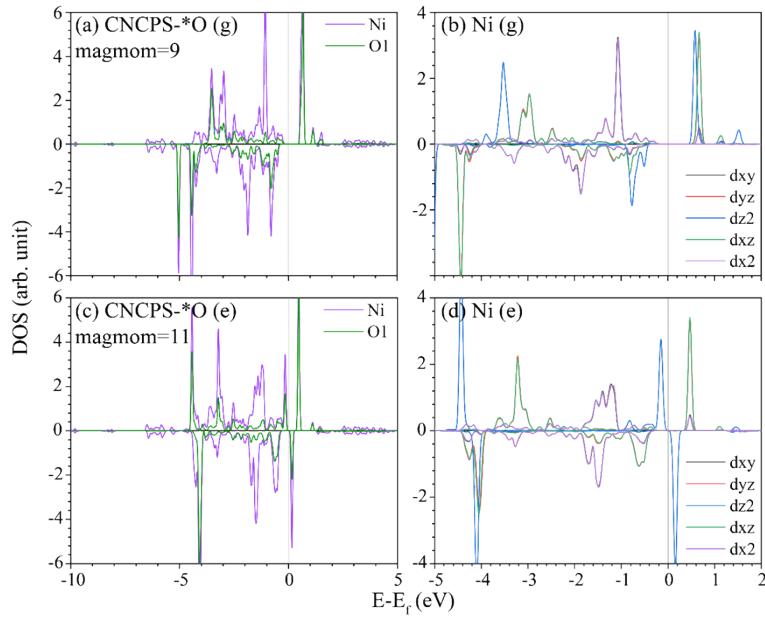
Figure S21. PDOSs for (a) Ni and O1 atoms and (b) *d* orbitals of Ni for CNCPS-*O (+9). PDOSs for (c) Ni and O1 atom and (d) *d* orbitals of Ni for CNCPS-*O (+11).
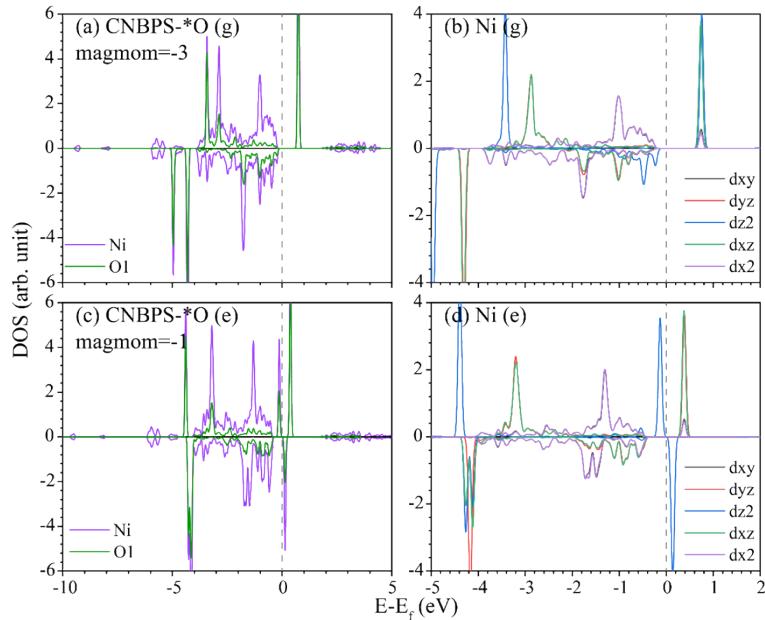


Figure S22. PDOSs for (a) Ni and O1 atoms and (b) *d* orbitals of Ni for ground-state CNBPS-*O (-3). PDOSs for (c) Ni and H atom and (d) *d* orbitals of Ni for excited-state CNBPS-*O (-1).
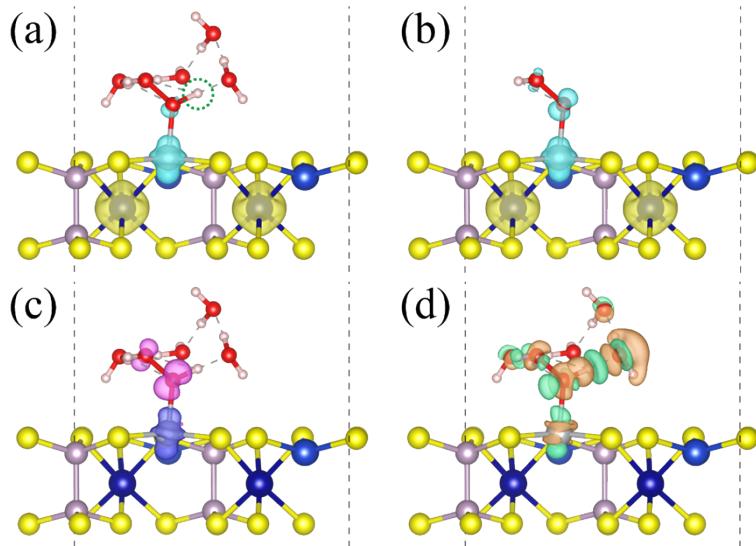
Figure S23. Spin densities of (a) CNCPS-*OOH+$H_9O_4$ and (b) CNCPS-*OOH⁻. Both isosurfaces in (a) and (b) are 0.02 e/Å³. The yellow and cyan represents spin up and down, respectively. Differential (c) spin and (d) charge densities of CNCPS-*OOH+$H_9O_4$. The pink and blue indicate that the magnetic moment gets bigger and smaller, orange and green denote charge accumulation and loss, respectively. Both isosurfaces in (a) and (b) are 0.005 e/Å³. The adsorbed H is circled in (a).

CNXPS-*OH intermediate
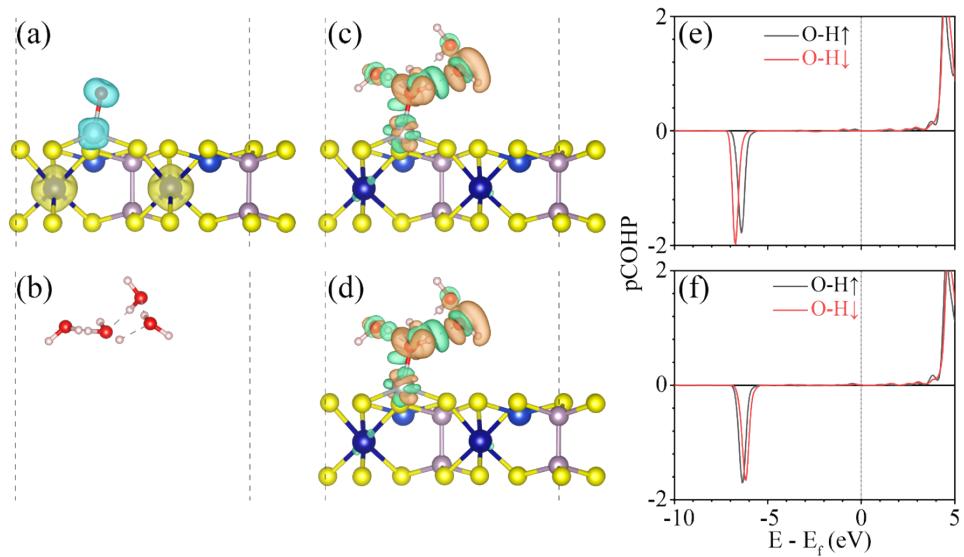


Figure S24. Spin density of (a) CNCPS-*O⁻ and (b) $H_9O_4^+$. Differential charge density of (c) ground-state CNCPS-*O+$H_9O_4$ (+9) and (d) excited-state CNCPS-*O+$H_9O_4$ (+11). COHP analysis for O-H bond of (e) ground-state CNCPS-*O+$H_9O_4$ (+9) and (f) excited-state CNCPS-*O+$H_9O_4$ (+11). The yellow and cyan represents spin up and down, orange and green denote charge accumulation and

loss, respectively. Isosurfaces are 0.02 e/Å$^3$ in (a) and (b), and 0.005 e/Å$^3$ in (c) and (d).
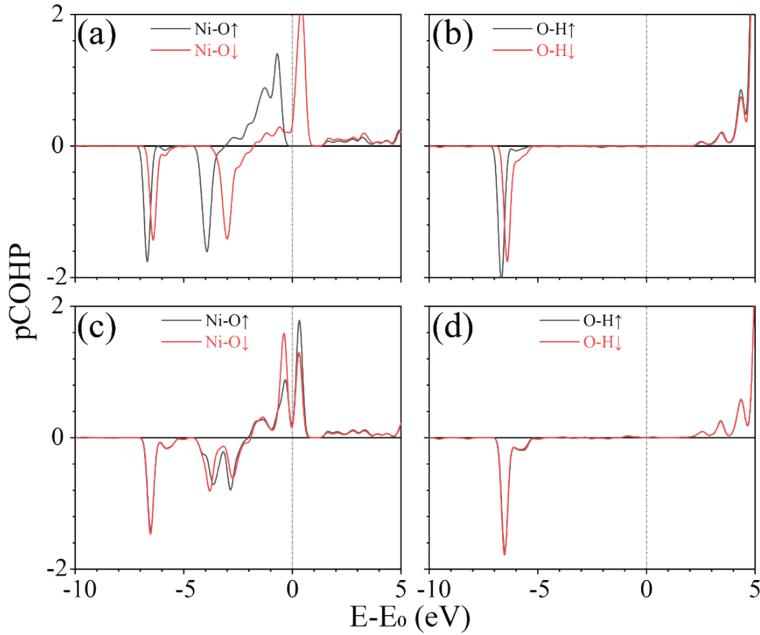


Figure S25. COHP analysis for (a) Ni-O, (b) O-H bond of ground-state CNBPS-*OH (+2). COHP analysis for (c) Ni-O, (d) O-H bond of excited-state CNBPS-*OH (0).
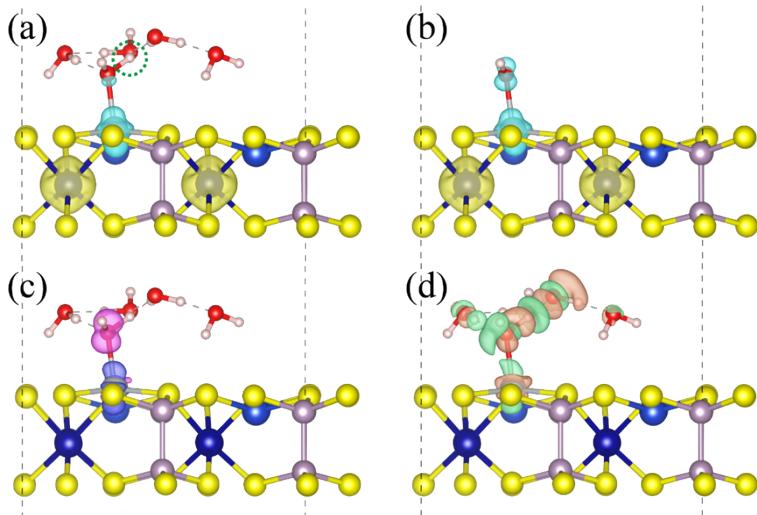


Figure S26. Spin densities of (a) ground-state CNCPS-*OH+H$_9$O$_4$ (+11) and (b) CNCPS-*OH$^-$ (+11). Isosurfaces are 0.02 e/Å$^3$. The yellow and cyan represents spin up and down, respectively. Differential (c) spin and (d) charge densities of ground-state Ni-*OH+H$_9$O$_4$ (+11). The pink and blue indicate that the magnetic moment gets bigger and smaller, respectively. The orange and green denote charge accumulation and loss, respectively. The isosurfaces are 0.005 e/Å$^3$. The adsorbed H is circled in (a).

References

1.   Nørskov, J. K.; Rossmeisl, J.; Logadottir, A.; Lindqvist, L.; Kitchin, J. R.; Bligaard, T.; Jónsson, H., Origin of the Overpotential for Oxygen Reduction at a Fuel-Cell Cathode. *The Journal of Physical Chemistry B* **2004,** *108* (46), 17886-17892.

2.   Malko, D.; Lopes, T.; Symianakis, E.; Kucernak, A. R., The intriguing poison tolerance of non-precious metal oxygen reduction reaction (ORR) catalysts. *Journal of Materials Chemistry A* **2016,** *4* (1), 142-152.

3.   Jung, J.-I.; Jeong, H. Y.; Lee, J.-S.; Kim, M. G.; Cho, J., A Bifunctional Perovskite Catalyst for Oxygen Reduction and Evolution. *Angew. Chem.* **2014,** *126* (18), 4670-4674.

4.   Chen, Y.; Ji, S.; Zhao, S.; Chen, W.; Dong, J.; Cheong, W.-C.; Shen, R.; Wen, X.; Zheng, L.; Rykov, A. I.; Cai, S.; Tang, H.; Zhuang, Z.; Chen, C.; Peng, Q.; Wang, D.; Li, Y., Enhanced oxygen reduction with single-atomic-site iron catalysts for a zinc-air battery and hydrogen-air fuel cell. *Nature Communications* **2018,** *9* (1).

5.   Cai, H.; Chen, B.; Zhang, X.; Deng, Y.; Xiao, D.; Ma, D.; Shi, C., Highly active sites of low spin FeIIN4 species: The identification and the ORR performance. *Nano Research* **2021,** *14* (1), 122-130.

6.   Yan, B.; Krishnamurthy, D.; Hendon, C. H.; Deshpande, S.; Surendranath, Y.; Viswanathan, V., Surface Restructuring of Nickel Sulfide Generates Optimally Coordinated Active Sites for Oxygen Reduction Catalysis. *Joule* **2017,** *1* (3), 600-612.

7.   Huang, K.; Liu, J.; Wang, L.; Chang, G.; Wang, R.; Lei, M.; Wang, Y.; He, Y., Mixed valence CoCuMnOx spinel nanoparticles by sacrificial template method with enhanced ORR performance. *Appl. Surf. Sci.* **2019,** *487*, 1145-1151.

8.   Li, H.; Wang, J.; Qi, R.; Hu, Y.; Zhang, J.; Zhao, H.; Zhang, J.; Zhao, Y., Enhanced Fe 3d delocalization and moderate spin polarization in Fe Ni atomic pairs for bifunctional ORR and OER electrocatalysis. *Applied Catalysis B: Environmental* **2021,** *285*, 119778.

9.   Li, F.; Ai, H.; Shen, S.; Geng, J.; Ho Lo, K.; Pan, H., Two-Dimensional Dirac Nodal Line Carbon Nitride to Anchor Single-Atom Catalyst for Oxygen Reduction Reaction. *ChemSusChem* **2022**.

10. Chen, X.; Hu, R., DFT-based study of single transition metal atom doped g-C3N4 as alternative oxygen reduction reaction catalysts. *Int. J. Hydrogen Energy* **2019,** *44* (29), 15409-15416.

11. Qin, M.; Meng, X.; Wang, W., Analysis on the secondary active site of FeN4-graphene for oxygen reduction reaction by DFT calculation. *Chem. Phys. Lett.* **2021,** *765*, 138321.

12. Chen, X.; Zhang, Y.; Hu, R.; Qing, S.; Zhang, H., DFT study of C2N-supported Ag3M (M = Cu, Pd, and Pt) clusters as potential oxygen reduction reaction catalysts. *Chem. Eng. Sci.* **2021,** *239*, 116642.

13. Modak, B.; Srinivasu, K.; Ghosh, S. K., Exploring metal decorated Porphyrin-like Porous Fullerene as catalyst for oxygen reduction reaction: A DFT study. *Int. J.*

*Hydrogen Energy* **2017,** *42* (4), 2278-2287.